

1 *Supplementary Information*

**A transient CGCM simulation of the past 3 million  
years**

Kyung-Sook Yun<sup>1,2\*</sup>, Axel Timmermann<sup>1,2\*</sup>, Sun-Seon Lee<sup>1,2</sup>, Matteo Willeit<sup>3</sup>, and  
Andrey Ganopolski<sup>3</sup>, and Jyoti Jadhav<sup>1,2</sup>

<sup>1</sup>Center for Climate Physics, Institute for Basic Science (IBS), Busan, Republic of  
Korea

<sup>2</sup>Pusan National University, Busan, Republic of Korea

<sup>3</sup> Potsdam Institute for Climate Impact Research, Potsdam, Germany

2

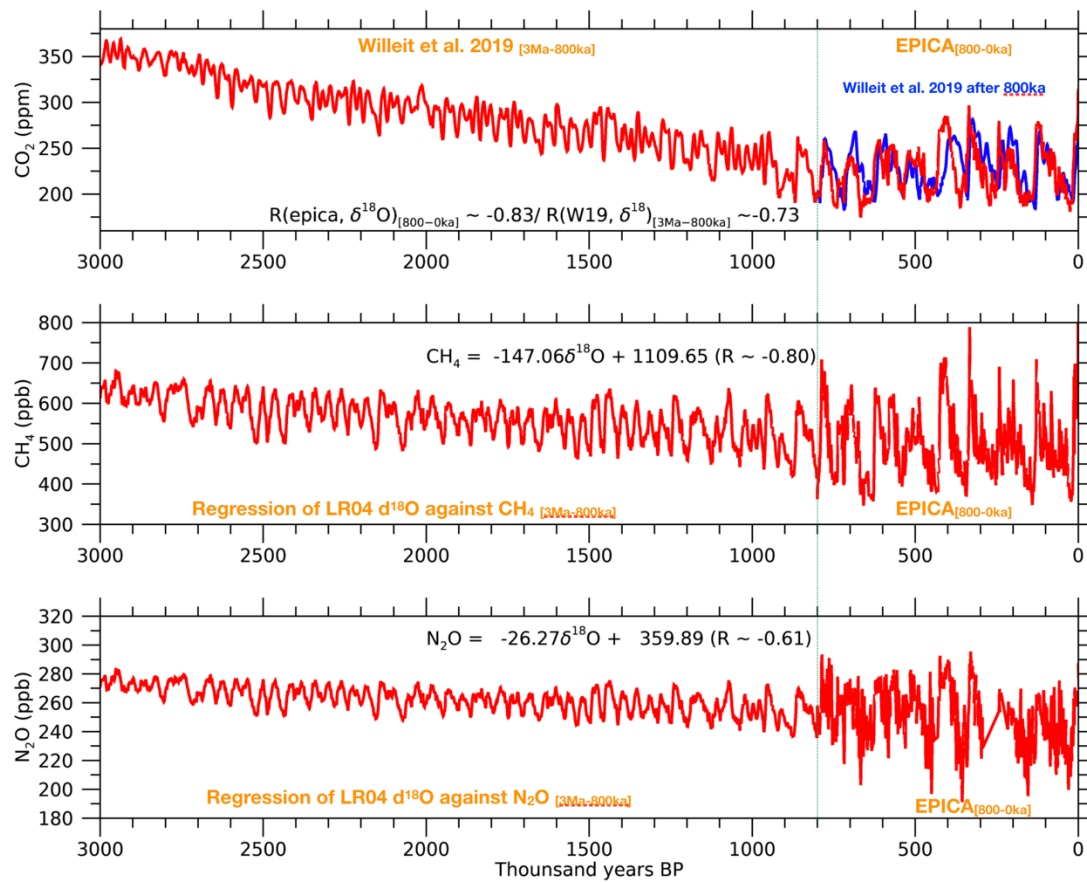
3

4

5

6

7

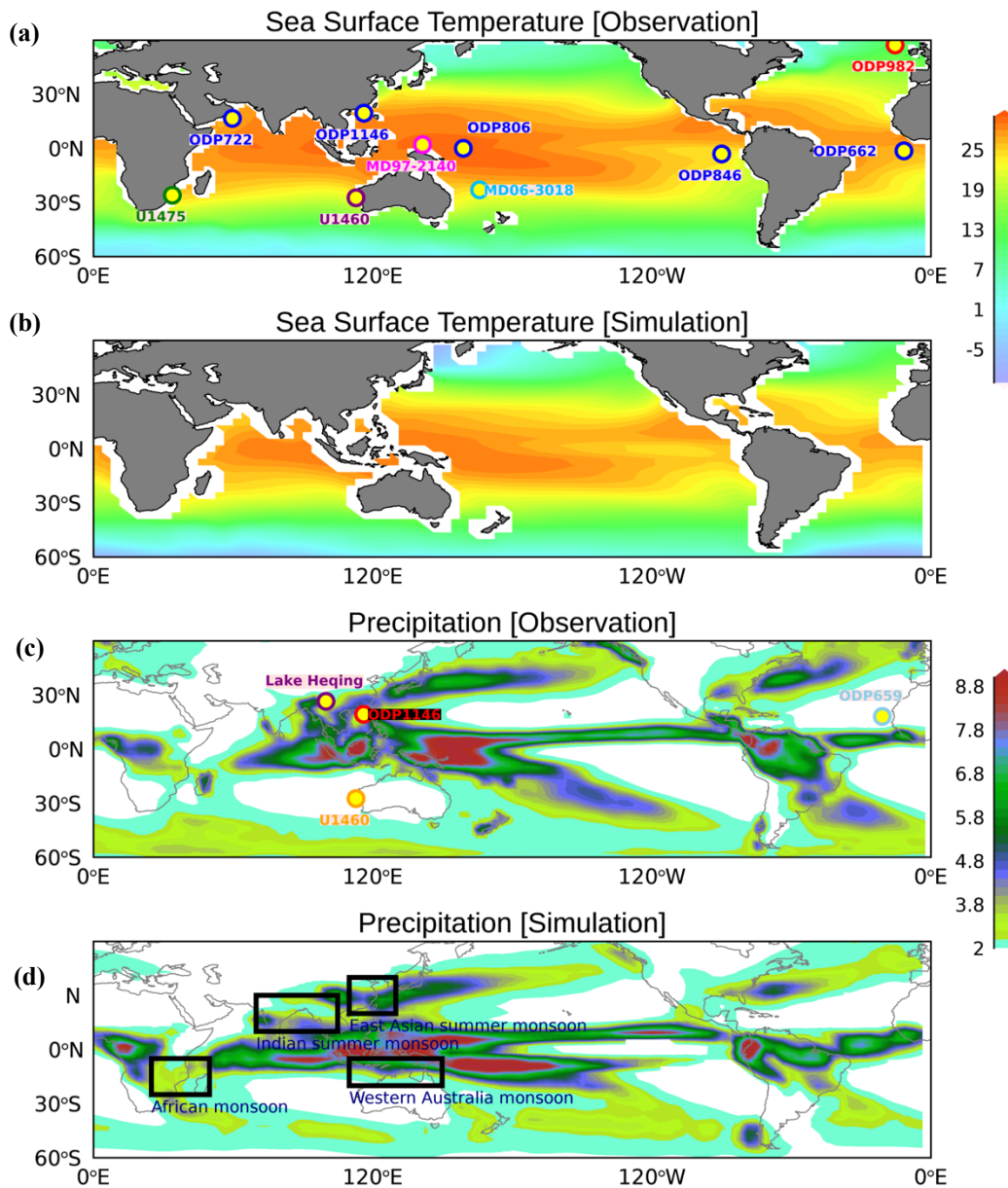


8

9 **Figure S1 | Greenhouse-gases forcing.** (a) Reconstructed CO<sub>2</sub> forcing (red) by combining two datasets of  
 10 the European Project for Ice Coring in Antarctica (EPICA) Dome ice core data (Lüthi et al. 2008) after  
 11 800ka and Willeit et al. (2019) before 800ka. Blue line indicates the CO<sub>2</sub> forcing from Willeit et al. (2019).  
 12 (b-c) Reconstructed (b) CH<sub>4</sub> and (c) N<sub>2</sub>O forcings by combining two datasets of EPICA CH<sub>4</sub> (Loulergue et  
 13 al. 2008) and N<sub>2</sub>O (Spahni et al. 2005) data after 800ka and regression model before 800ka. Here, the  
 14 regression was conducted using the linear relationship between LR04 stack (Lisiecki and Raymo 2005) and  
 15 the greenhouse-gases during the EPICA 800 kyr. The regression coefficients were displayed by equation of  
 16 each panel.

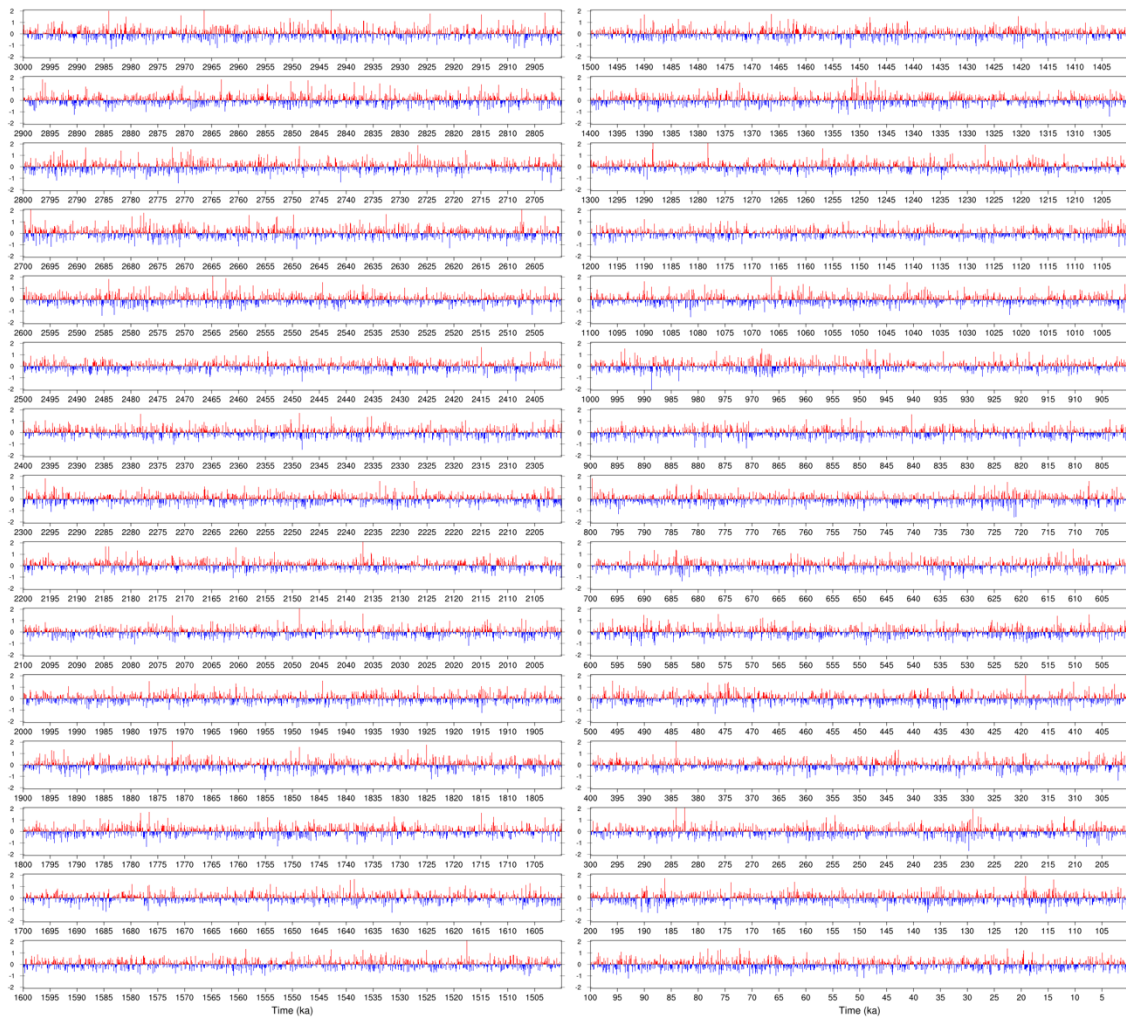
17

18



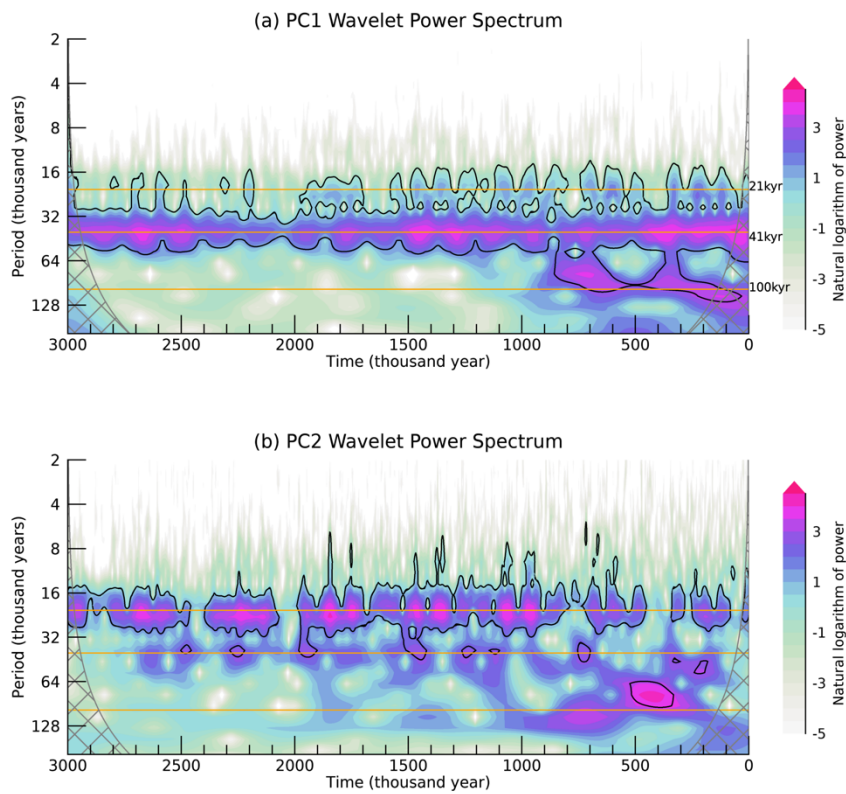
19  
 20  
 21  
 22  
 23  
 24  
 25  
 26  
 27  
 28

**Figure S2 | SST and precipitation pattern.** (a) Observed SST pattern during 1979-2008 from ERSST5 and proxy locations used in this study. (b) Simulated SST pattern over the entire 3Myr. (c) Observed precipitation pattern during 1979-2008 from GPCP and proxy locations. (d) Simulated precipitation pattern over the 3Myr and monsoon domains used in this study.



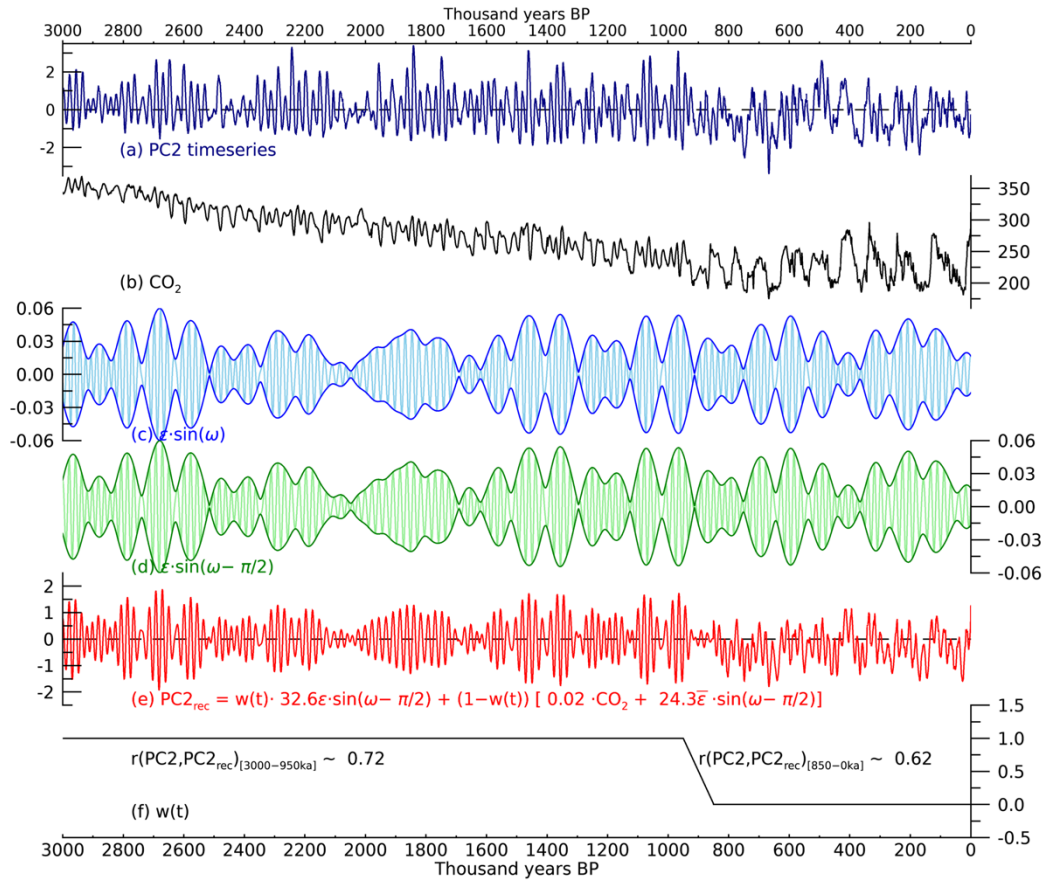
29  
30  
31  
32

**Figure S3 | Monthly ENSO variability.** Timeseries of Niño 3 index defined as 1.5-7-year band-pass filtered Niño 3 SST.



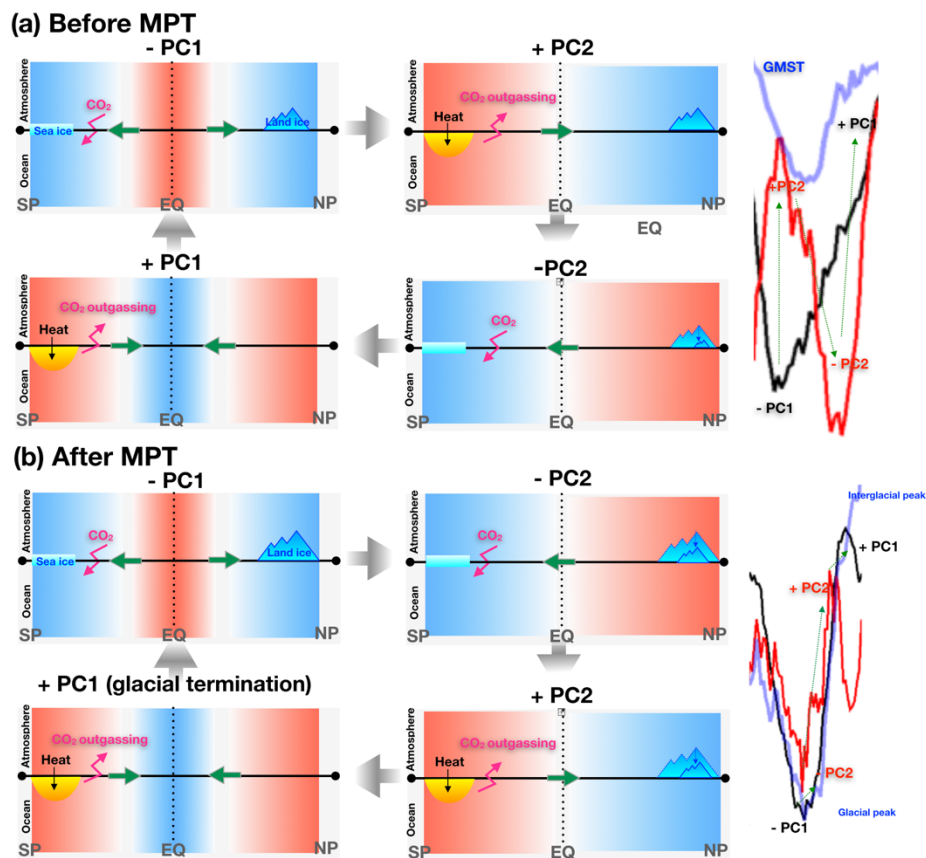
33  
 34  
 35  
 36  
 37  
 38  
 39  
 40  
 41  
 42  
 43  
 44  
 45  
 46  
 47  
 48  
 49

**Figure S4 | Wavelet power spectrum of PCs of two dominant MHT modes.** The wavelet power spectrum of (a) PC1, and (b) PC2. The black contour indicates the value significant at the 95% confidence level. The horizontal orange lines show 21-kyr (precession), 41-kyr (obliquity), and 100-kyr (eccentricity) periods.



50  
 51  
 52  
 53  
 54  
 55  
 56  
 57  
 58  
 59  
 60  
 61

**Figure S5 | A simple model for reconstructing PC2 time series using eccentricity-modulated precession and CO<sub>2</sub>.** (a) Original PC2 time series, (b) CO<sub>2</sub> forcing, (c) eccentricity (blue)-modulated precession (sky blue) variability. (d) 90° out-of-phase precession variability, (e) reconstructed PC2 time series using 90° out-of-phase precession and CO<sub>2</sub> forcing, and (f) weight function in the reconstruction. The coefficients in (e) are obtained using a simple regression model against the PC2 time series.



62

63 **Figure S6 | PC1-PC2 cycle and the potential feedback with carbon cycle.** The cycle of PC1 and PC2 (a)  
 64 before the MPT and (b) after the MPT. Before the MPT, the negative PC1 tends to be followed by the  
 65 positive PC2 and it becomes the other way around. Meanwhile, after the MPT, the negative PC1 tends to  
 66 be followed by the negative PC2 during the glacial peak. The transition into positive phases of PC2 and  
 67 PC1 is concurrent with the glacial termination. The negative phases of PC1 and PC2 are likely to enhance  
 68 the Southern Ocean CO<sub>2</sub> sequestration into the ocean, associated with the sea ice/carbon cycle feedback  
 69 (Stein et al. 2020). By contrast, the positive phases of PC1 and PC2 are related to the Southern Ocean  
 70 warming and the enhanced CO<sub>2</sub> leak outgoing into the atmosphere. Here, blue (red) shading and green  
 71 arrow show an anomalous cooling (warming) and direction of heat transport.

72

73

74

75

76

77

78

79

80 **References**

81 Lisiecki, L. E., and M. E. Raymo, 2005: A Pliocene-Pleistocene stack of 57 globally  
82 distributed benthic  $\delta^{18}\text{O}$  records. *Paleoceanography*, **20**.

83 Louergue, L., and Coauthors, 2008: Orbital and millennial-scale features of atmospheric  
84  $\text{CH}_4$  over the past 800,000 years. *Nature*, **453**, 383-386.

85 Lüthi, D., and Coauthors, 2008: High-resolution carbon dioxide concentration record  
86 650,000–800,000 years before present. *Nature*, **453**, 379-382.

87 Spahni, R., and Coauthors, 2005: Atmospheric Methane and Nitrous Oxide of the Late  
88 Pleistocene from Antarctic Ice Cores. *Science*, **310**, 1317-1321.

89 Stein, K., A. Timmermann, E. Y. Kwon, and T. Friedrich, 2020: Timing and magnitude of  
90 Southern Ocean sea ice/carbon cycle feedbacks. *Proceedings of the National Academy of  
91 Sciences*, **117**, 4498-4504.

92 Willeit, M., A. Ganopolski, R. Calov, and V. Brovkin, 2019: Mid-Pleistocene transition  
93 in glacial cycles explained by declining  $\text{CO}_2$  and regolith removal. *Sci Adv*, **5**.

94